Experimental measurement of gain and loss in a microcavity laser

Sang Hun Lee*
Department of Physics, Seonam University, Namwon, Jeonbuk 590-711, Republic of Korea

Myung-Woon Kim, Sunghwan Rim, and Chil-Min Kim†
Acceleration Research Center for Quantum Chaos Application, Sogang University, Seoul 121-741, Republic of Korea

Jong Hoi Kim and Kwang Ryung Oh
IT Convergence and Components Laboratory ETRI, Yusung-Gu, Daejeon 305-700, Republic of Korea
(Received 12 November 2011; published 27 February 2012)

In a microcavity laser, it is known that the quality factor obtained experimentally is much less than the one obtained numerically. This quality factor degradation in experiment is caused by various effects, such as absorption, surface roughness, flatness of the ridge boundary, and curvature. To understand the quality-factor degradation we obtain the gain and the internal loss coefficient in an elliptic microcavity laser. In the experiment, we take a triangular orbit. To confirm the triangular orbit, we measure the mode spacing and estimate the emission direction by including the Fresnel filtering. By using the Fourier transform analysis, we obtain the loss and gain coefficients because the triangular orbit can be regarded as a Fabry-Perot resonator due to the incidence angle. The obtained loss for our microcavity laser is larger than the one caused by material absorption, which is due to environmental losses, such as surface roughness and flatness of the ridge boundary.

DOI: 10.1103/PhysRevA.85.023839 PACS number(s): 42.55.Sa, 42.55.Px, 05.45.Mt

I. INTRODUCTION

In a deformed microcavity laser, resonances and their emission directions have been intensively studied because the cavity has high potentiality in applications for optoelectronic circuits. Most recent studies are focused on high-quality-factor resonance modes, which emit unidirectionally in cavities with spiral [1], rounded-isosceles-triangle [2], annular [3], limaçon [4], gibbous [5], and ellipse-with-notch shapes [6] and two jointed half ellipses [7]. Along with these regular scarred resonances, two special kinds of resonance, a quasiscar [8–10] and a scarlike [11] resonance, have attracted much attention because they appear only in an open system. Quasiscar and scarlike resonances were experimentally verified in spiral-shaped [12] and ellipse-shaped microcavity lasers [13], respectively.

Regarding a scarlike mode observed in an elliptic microcavity laser, the cavity can be considered as a deformed cavity from a circle while the integrability of the underlying classical ray dynamics is preserved. The important feature of the ray dynamics of an elliptic cavity in comparison with a circular cavity is that there exist two different types of motion [14]: One is a bouncing-ball-type mode and the other is a whispering-gallery mode. The scarlike resonance modes show localized intensity patterns on a specific periodic orbit underlying in the corresponding classical ray dynamics. This phenomenon is something unexpected because the ray dynamics of the elliptic cavity is integrable and the resonance modes of the corresponding wave mechanics are believed to be supported by the underlying resonant tori rather than by a specific periodic orbit according to the usual ray and wave correspondence. In order to explain the wave phenomenon of localized modes for systems with an integrable closed counterpart, Unterhinninghofen *et al*. have developed a semiclassical extension of the ray dynamics including the Goos-Hänchen shift [15]. It is therefore quite important to study the impact of these scarlike modes on emission properties of an elliptic cavity. The necessity of this study is one motivation for the experiment we perform in this paper.

In an open system such as a semiconductor microcavity, there exists no true bound state due to the loss on the cavity boundary. In a microcavity laser, the intensity of light increases as the light travels inside of the cavity when the cavity is connected to an external source. Hence the resonance mode usually expected to have a short lifetime can last a long time because of the gain effect from the external excitation. However, the intensity also decays due to the inherent absorption of the cavity material and the transmission through the boundary. In a microcavity laser, in addition to these losses, surface roughness, flatness, and curvature on the boundary can work as losses degrading the quality factor because the cavity size is so small. Hence the measurement of the loss and the gain in a certain periodic orbit can help us understand the optical properties of a periodic orbit. This expectation is another motivation for our study.

Our experiments are performed by using a highly deformed elliptic microcavity laser, which generates various scarlike resonance modes of triangular, bow-tie, double-bow-tie, and triple-bow-tie orbits below the laser threshold [13]. Among them, we attend to a resonance mode of a triangular orbit, whose incidence angle is less than the critical angle, for measurement of the gain and the loss because it can be regarded as the mode in a Fabry-Perot resonator. In Sec. II, the path length is obtained from the mode spacing to estimate the periodic orbit. From the path length, we confirm the triangular scarlike mode. In Sec. III, the emission directions are calculated by including the Fresnel filtering [16,17] to understand the emission direction of a triangular scarlike

*linuet@naver.com
†chmkim@sogang.ac.kr

mode. We also show that the emission directions including the Fresnel filtering well agree with the emission direction measured near the major axis. In Sec. IV, we measure the loss and the gain of the InGaAsP/InP microcavity by using the Fourier transform analysis [18,19]. We compare the experimental results with the values obtained by different measurement methods [20–23] and discuss them.

II. EXPERIMENTAL SETUP AND SPECTRUM

An elliptic InGaAsP/InP multiple-quantum-well microcavity laser, whose minor axis radius is 30 μm and whose aspect ratio is $b/a = 0.3179$, is fabricated, where a and b are the radii of the major and the minor axes, respectively. The fabrication procedure and parameters are the same as in Refs. [12,24]. To measure the emission spectrum, we use a lensed optical fiber whose core and clad diameter are 8 and 125 μm, respectively. The input facet of the lensed fiber is a cone type whose angle is 70°, and the input facet of the fiber core is spherical, with a radius of 15 μm. The launched emission intensity is measured with a power meter (Newport 818-IR) connected to a multifunction optical meter (Newport 1835-C). The emission spectrum is measured with an optical spectrum analyzer (Agilent 86142B) as we increase the injection current. The current is controlled with a laser diode controller (Lightwave LDC-3744B) at room temperature ($T = 20\,^{\circ}$C).

Figure 1(a) is the experimental setup, showing an elliptic microcavity laser, the stylus (as an anode), and the lensed optical fiber for measurement of the emission. Figure 1(b) shows triangular periodic orbits developed inside the elliptic microcavity laser. The length of the orbit is $\mathcal{L} = 387.26\,\mu$m. The incident angles at three reflecting points, $P_1 = (94.243, 1.552)$, $P_2 = (94.243, -1.552)$, and $P_3 = (0, -30)$ in Cartesian coordinates, are about 9.26° for P_1 and P_2 and 71.49° for P_3. At point P_3, total internal reflection occurs because the incident angle is larger than the critical angle, $\theta_c = 17.88^{\circ}$, for the effective refractive index of $n_e = 3.258$, where n_e is obtained by the beam propagation method. At point P_1, two transmitted lights, E_1 and E_2, are caused by the clockwise and the counterclockwise traveling waves, respectively. The

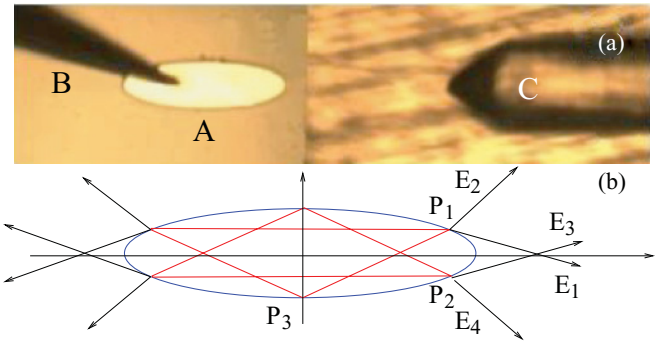

FIG. 1. (Color online) (a) Experimental setup: A is the elliptic microcavity laser, B is the stylus as an anode, and C is a lensed optical fiber for measurement of the emission. (b) Diagram of triangular orbits developed inside the elliptic microcavity, where the distance of points P_1 and P_2 from the major axis is exaggerated for clarity.

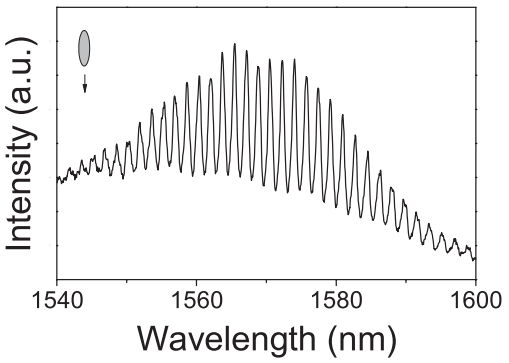

FIG. 2. Emission spectrum measured near the major vertex at a current of $I = 50$ mA below the laser threshold current ($I_{\rm th} \simeq 65$ mA).

emission direction of E_1 and E_2 is 31.6° with respect to the outward normal when the Fresnel filtering effect [16,17] is not taken into account.

Figure 2 is the measured spectrum near the major vertex at the injection current $I = 50$ mA, which is less than the threshold current for laser emission ($I_{\rm th} \sim 65$ mA). Figure 2 shows that the average mode spacing $\Delta\lambda$ is 1.71 ± 0.05 nm in the range from 1565 to 1575 nm for the mean wavelength of about 1569.71 nm. When we consider the mode spacing of $\Delta\lambda$ and the group refractive index of $n_g = 3.68$ [13], the orbit length $\mathcal{L}$ inside the elliptic microcavity is 390.8 μm within 2.8% error. This experimentally obtained orbit length is very close to the length of the triangular orbit of 387.26 μm within a deviation of 0.9%. This value is quite different from the orbit length of the bow-tie resonance mode of 398.1 μm. Indeed, the emission of the triangular mode is measured around the major axis, as in Ref. [13]. The lasing emission of the bow-tie mode is also measured around the major axis, as in Ref. [13]. Nevertheless, the emission direction of the bow-tie mode is still about ±25° from the major axis, as shown in Ref. [13]. Actually, we can detect the weak emission of the bow-tie mode because of the acceptance angle of the fiber, but the intensity is weaker than the intensity of the triangular mode. Hence the emission around the major axis is the triangular mode. Also the length of the triangular orbit is much shorter than that of the bow-tie orbit of 398.1 μm. In the next section, we describe the emission direction of the triangular mode by including the Fresnel filtering effect.

III. EMISSION DIRECTION

When a beam with a Gaussian angular distribution is incident to the boundary inside the cavity, a part of the light, whose incident angle is larger than the critical angle, is totally reflected with an evanescent wave. The other part of the light in the angular distribution is reflected and transmitted across the boundary according to Snell's law. Hence the direction of the outward beam field is shifted from what is expected by Snell's law. This effect is known as Fresnel filtering [16,17].

When a beam field E_i is incident to the inward boundary with a Gaussian angular distribution as shown in Fig. 3, the

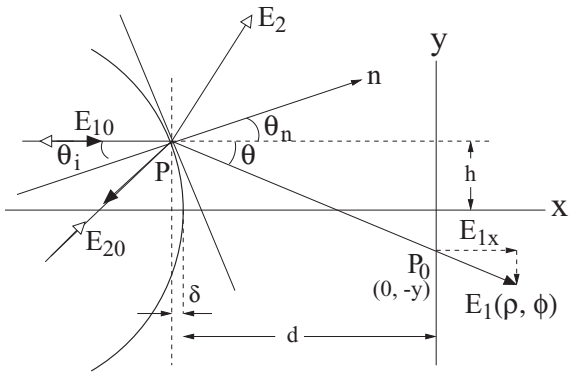

FIG. 3. Diagram of the calculation including the Fresnel filtering. P_0 is the observation point on the y axis, and P is the emission point on the boundary. There are two refracted beam fields, E_1 and E_2, at one reflected point due to clockwise and counterclockwise propagation directions. n and θ_n are the outward normal direction and the angle from the x axis at point P, respectively. θ is the angle between the observation point P_o and the x axis. δ and h are the differences of x and y components between the bouncing point and the vertex point, respectively. d is the distance between the vertex and the y axis.

refracted asymptotic far field E is given as follows [16]:

$$E = \frac{E_0\Omega}{\sqrt{2i\rho\Omega/n_e}} \frac{\left[\sqrt{1-s_o^2}\cos\phi\right]}{\sqrt{n_e^2-\sin^2\phi}} T(s_o)G(s_o)\exp(i\rho\Omega/n_e)\,, \tag{1}$$

$$T(s_o) = \frac{2n_e\sqrt{n_e^2-\sin^2\phi}}{\mu\sqrt{n_e^2-\sin^2\phi}+n_e^2\sqrt{1-\sin^2\phi}}\,, \tag{2}$$

$$G(s) = \exp[-(\Omega/2)^2 s^2 + i\Omega\sqrt{1-s^2}z_o]\,, \tag{3}$$

$$s_o(\phi) = \left[\sin\phi\cos\theta_i - \sin\theta_i\sqrt{n_e^2-\sin^2\phi}\right]/n_e\,, \tag{4}$$

where $P_o(\rho,\phi)$ is the observation point in the polar coordinate attached to the boundary, θ_i is the incidence angle, μ is the polarization factor of 1 (or n_e) for TE (or TM), and $\Omega = n_e k_o w$ is the dimensionless width of the incidence Gaussian beam. Here w is the minimum beam waist at a distance z_o from the interface, and k_o is the wave number in free space.

When a certain periodic orbit is developed inside the microcavity, there are two emission directions at one reflected point P due to clockwise and counterclockwise propagation directions. In the case of the triangular orbit in an elliptic microcavity, the total field E at the observation point P_o is a vector sum of E_1, E_2, E_3, and E_4, as shown in Fig. 1(b). The x component of the total field E on point P_o is given by

$$E_x = E_{1x} + E_{2x} + E_{3x} + E_{4x}\,. \tag{5}$$

In this orbit, fields E_3 and E_4 and fields E_1 and E_2 are symmetric with respect to the x axis, respectively. Field E_1 at point P_o is calculated numerically by using the Eqs. (1)–(4) with consideration of the following relations:

$$\phi = \theta + \theta_n\,, \tag{6}$$

$$\rho = (d+\delta)/\cos\theta\,, \tag{7}$$

$$\theta = \tan^{-1}[(-y+h)/(d+\delta)]\,, \tag{8}$$

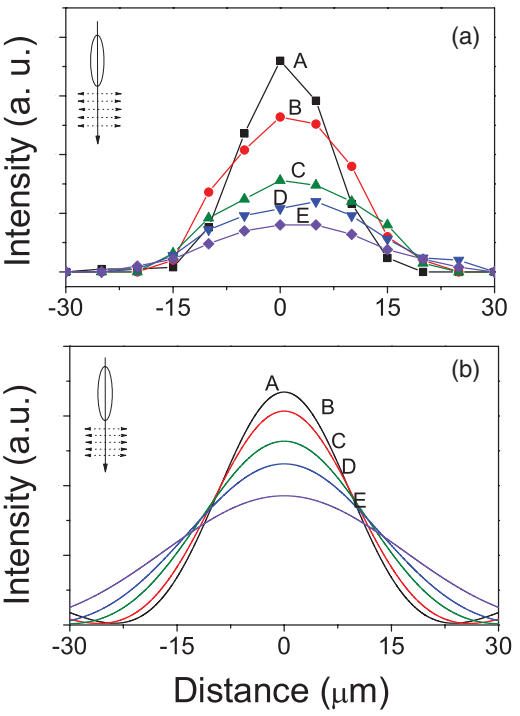

FIG. 4. (Color online) Emission intensity distribution depending on the distance. (a) The measured intensity distribution depending on the distance when the injection current is 50 mA. The curves from A through E are the emission intensity depending on the position on the y axis when the distance is 55, 60, 70, 80, and 100 μm away from the major vertex, respectively. (b) Numerically obtained distributions of a triangular orbit including the effect of Fresnel filtering when the distance is the same as in (a).

where θ_n is the angle between the x axis and the outward normal at point P. θ is the angle between the observation point P_o and the x axis. δ and h are the x and y component differences between the bouncing point and the vertex point, respectively, and d is the distance between the vertex and the y axis. Fields E_2, E_3, and E_4 can be calculated similarly.

Figure 4(a) is the measured intensity distributed on the y axis depending on the distance as shown by the inset. The curves from A to E are the intensity distribution when the distance is 55, 60, 70, 80, and 100 μm away from the major vertex, respectively, at the injection current of $I = 50$ mA. Figure 4(b) is the calculated result of the intensity distribution including the Fresnel filtering effect for the triangular orbit at the same distances as in Fig. 4(a). The fitted parameters are $z_o = 2.5$ μm and $\Omega = 8.0742$. Due to the Fresnel filtering effect, the emission direction is rotated about 6° to the outward normal from the direction expected according to Snell's law, 31.6°. The measured direction is similar to the calculated one. Figure 4 shows the maximum intensity on the major axis. Hence we can measure the emission of the triangular orbit in the major-axis direction.

IV. LOSS AND GAIN COEFFICIENTS

Measurement of the loss and gain coefficients is useful for understanding the quality-factor degradation and the optical property of a microcavity laser. To obtain the loss and gain

coefficients, first, the reflectance R should be precisely determined by considering the polarization state of the emission. From the measurement of the emission polarization, we find that the emission is composed of about 90% p polarization and about 10% s polarization. The reflectance R is about 0.226 at the reflection point P_1 because the incident angle is $\theta_i = 9.26^\circ$. On determination of the reflectance, we carefully consider the Gaussian angular distribution of the incident wave. At reflection point P_1, we approximately obtain the radius of the curvature, which is about 41.383 μm. When we apply Hentschel's [25] and Lee's [7] theoretical results, the reflectance is about 0.22583, while the reflectance due to the Fresnel equation is about 0.22582. The difference is less than 0.01%.

Because of the reflectance, which is $R < 1.0$, the triangular periodic orbit can be considered as a Fabry-Perot-type resonator. To obtain the loss and the gain we obtain Fourier transform spectra depending on the injection current. The adjacent peak-amplitude ratio r in a Fourier transform spectrum contains the information of the propagation loss-gain K at a given injection current in a Fabry-Perot-type laser because of the relation of $r = I_{i+1}/I_i = Re^{-KL}$, where I_{i+1} and I_i are the $(i+1)$th and ith peaks in the transformed spectrum, respectively, and L is the cavity length [18,19,26]. When a light travels along a path periodically, the Fourier transform spectrum $I(x_d)$ of the emission spectrum is given as follows:

$$I(x_d) = |1 - Re^{2i\psi}|^2 \times \sum_{m=0}^{\infty}\sum_{l=0}^{\infty} \frac{[R^{(l+m)}e^{-2i\psi(l-m)}]}{\{\kappa L(l+m+1)+i[\pi x_d + n_g L(l-m)]\}}, \tag{9}$$

where x_d is the Fourier transform pair of the wave number k, l and m are the integers, κ is the imaginary part of the complex refractive index, ψ is the effective phase change of the light due to the reflection, and R is the reflectance at the reflection point. Here the imaginary part of the complex wave number is given by $\mathrm{Im}[\mathbf{k}] = k_o\kappa = \alpha/2$, where α is the total internal loss coefficient except for the loss due to the reflectance R [27].

Figure 5 shows the Fourier transform spectra of the emission spectra. The insets are the emission spectra when the injection currents are (a) $I = 38$ mA and (b) $I = 72$ mA. In our experiment, the distance of the input facet of the optical fiber, of which the direction is fixed on the direction of the major axis of the microcavity laser, is about 60 μm away from the major vertex. As the injection current is increased, the peak position and the mode spacing are almost maintained. Note that the resonance of the triangular orbit is not lased even if the injection current is larger than the threshold current for lasing the bow-tie resonance mode ($I_{\mathrm{th}} = 65$ mA). We measure the spectrum of the spontaneous emission up to $I = 78$ mA. In the transformed spectrum, since the first-order peak in Eq. (9) is at the position of $x_d = n_g\mathcal{L}/2\pi$, we can obtain the orbit length $\mathcal{L}$. The cavity length L in Eq. (9) corresponds to $\mathcal{L}/2$ in our cavity. As is shown in Figs. 5(a) and 5(b), since the adjacent peak-amplitude ratio $r = I_{i+1}/I_i$ increases as the injection current increases, we can determine the gain and the loss.

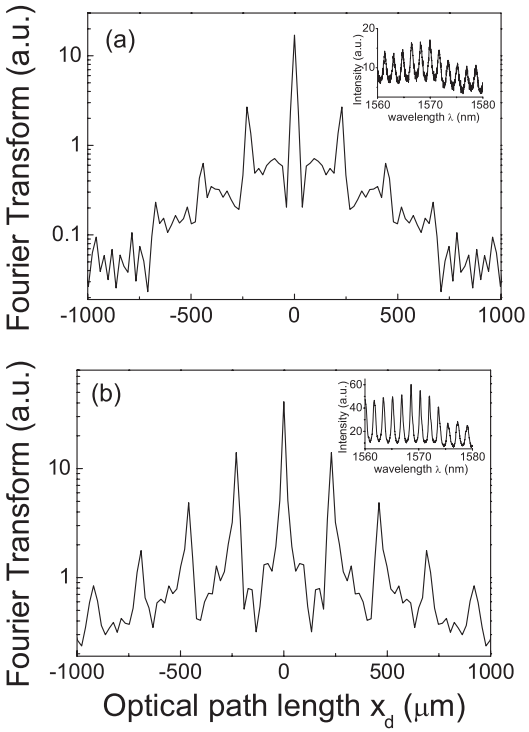

FIG. 5. Fourier transform spectra of the emission spectra (inset) from the elliptical microcavity when the injection currents are (a) 38 mA and (b) 72 mA. These spectra are measured in the direction of the major axis at a distance of about 60 μm away from the major vertex.

In the transformed spectra, we can obtain the gain and the loss from the following relation:

$$K = \alpha - \gamma(I), \tag{10}$$

where α is the total internal loss and γ is the gain. The gain γ has a dependency on the injection current I with the following form [19,21]:

$$\gamma(I) = \gamma_o \ln[I/I_c], \tag{11}$$

where γ_o is the gain coefficient of a microcavity laser. It is acceptable to treat the constant current I_c in Eq. (11) as a threshold current of the gain because the gain effect begins to emerge only when the current I is larger than I_c. When the injection current I is lower than I_c, only the effect of the loss α holds.

We measure r depending on the injection current from the Fourier transform spectra to find the current dependency of the propagation loss-gain K. Here we note that K is the sum of the loss and gain effects when the loss due to reflectance is not considered. Hence $K = 0$ does not imply the lasing threshold. The experiment is performed at the current from 10 to 78 mA with an interval of 5 mA. As shown in Fig. 6, when the injection current is less than 30 mA, there is no gain effect and only the internal loss exists. The dotted line implies the internal loss because below $I_c = 30$ mA the K is nearly constant. Above I_c, the emission begins to obtain gain and K decreases. This means that since $K = \alpha - \gamma(I)$, γ begins to increase. From this result, the total loss coefficient α and the constant current I_c can be determined. The values of α and I_c are 33 cm^{-1}

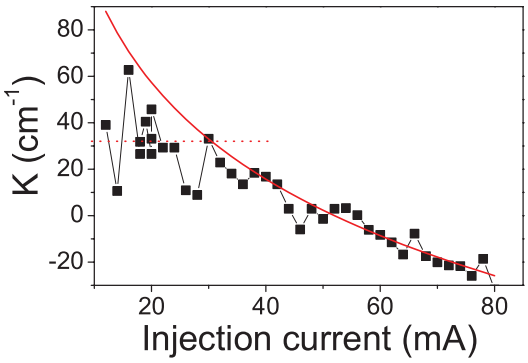

FIG. 6. (Color online) Propagation loss-gain coefficient K with the injection current I. $K = \alpha - \gamma_o \ln(I/I_c) = -2\ln(r/R)/\mathcal{L}$. r is the adjacent peak-amplitude ratio that is a function of the injection current I. The absorption and the gain coefficient, α and γ, are 33 and 60 cm^{-1}, respectively. The reflectance R at the bouncing point and the orbit length $\mathcal{L}$ of the triangular mode are 0.226 and 387.3 μm, respectively. The current constant I_c for the gain is 30 mA.

and 30 mA, respectively. The gain coefficient γ_o is obtained by logarithmic fitting, which is about 60 cm^{-1} (solid line). In the case of the Fabry-Perot-type laser diode with the same material of the InGaAsP/InP multiple-quantum-well structure, the internal loss α is about 16 cm^{-1} when the cavity length is longer than 1 mm [23,28]. In this case α is mainly caused by the inherent material absorption. In our microcavity laser, $\alpha =$ 33 cm^{-1} is much larger than α of the Fabry-Perot-type resonator due to inherent material absorption. We can understand that the loss is caused by surface roughness, flatness of the ridge boundary, and the curvature of the small-size microcavity. For this reason the total internal loss is larger than that of a Fabry-Perot-type resonator.

V. CONCLUSION

We observe the spectra of the spontaneous emission from the elliptic microcavity laser under the regime of the laser threshold. From the spectra, we obtain the modes that are mainly supported by the effectively isolated periodic orbit of a triangular orbit. To understand the quality-factor degradation, we measure the loss and gain coefficients of the InGaAsP/InP microcavity by regarding the triangular orbit as a Fabry-Perot resonator because the incidence angle is smaller than the critical angle. First, we confirm from the mode spacing and the analysis of the emission direction including the Fresnel filtering effect that the emission around the major-axis direction is a triangular orbit. From the Fourier transform analysis of the emission spectrum, we obtain the loss and gain coefficients. From the results, we understand that, in a small-size microcavity laser, the quality factor can be degraded in real systems due to various losses of surface roughness, flatness of the ridge boundary, and curvature as well as inherent material absorption.

ACKNOWLEDGMENTS

This study was supported by Acceleration Research (Center for Quantum Chaos Application) of MEST/NRF under the Contract No. 2011-0000299. We also acknowledge Dr. J. Cho and Dr. J. Lee for helpful discussions and calculation of the reflectance.

[1] G. D. Chern, H. E. Tureci, A. D. Stone, R. K. Chang, M. Kneissl, and N. M. Johnson, Appl. Phys. Lett. **83**, 1710 (2003).
[2] M. S. Kurdoglyan, S.-Y. Lee, S. Rim, and C.-M. Kim, Opt. Lett. **29**, 2758 (2004).
[3] J. Wiersig and M. Hentschel, Phys. Rev. A **73**, 031802(R) (2006).
[4] J. Wiersig and M. Hentschel, Phys. Rev. Lett. **100**, 033901 (2008).
[5] C. L. Zou, F.-W. Sun, C.-H. Dong, X.-W. Wu, J.-M. Cui, Y. Yang, G.-C. Guo, and Z.-F. Han, e-print arXiv:0908.3531v1.
[6] Q. J. Wang, C. Yan, N. Yu, J. Unterhinninghofen, J. Wiersig, C. Pflügl, L. Diehl, T. Edamura, M. Yamanishi, H. Kan, and F. Capasso, Proc. Natl. Acad. Sci. USA **107**, 22407 (2010).
[7] J. H. Lee, S. Rim, J. H. Cho, and C. M. Kim, Phys. Rev. A **83**, 033815 (2011).
[8] S.-Y. Lee, S. Rim, J.-W. Ryu, T.-Y. Kwon, M. Choi, and C.-M. Kim, Phys. Rev. Lett. **93**, 164102 (2004).
[9] S.-Y. Lee, S. Rim, J.-W. Ryu, T.-Y. Kwon, M. Choi, and C.-M. Kim, Phys. A **41**, 275102 (2008).
[10] J. Lee, S. Rim, J. Cho, and C. M. Kim, Phys. Rev. Lett. **101**, 064101 (2008).
[11] J. Wiersig, Phys. Rev. Lett. **97**, 253901 (2006).
[12] C. M. Kim, S. H. Lee, K. R. Oh, and J. H. Kim, Appl. Phys. Lett. **94**, 231120 (2009).
[13] C. H. Yi, S. H. Lee, M. W. Kim, J. Cho, J. Lee, S. Y. Lee, J. Wiersig, and C. M. Kim, Phys. Rev. A **84**, 041803(R) (2011).
[14] H. Waalkens, J. Wiersig, and H. R. Dullin, Ann. Phys. (NY) **260**, 50 (1997).
[15] J. Unterhinninghofen, J. Wiersig, and M. Hentschel, Phys. Rev. E **78**, 016201 (2008).
[16] H. E. Tureci and A. D. Stone, Opt. Lett. **27**, 7 (2002).
[17] N. B. Rex, H. E. Tureci, H. G. L. Schwefel, R. K. Chang, and A. D. Stone, Phys. Rev. Lett. **88**, 094102 (2002).
[18] D. Hofstetter and R. L. Thornton, Opt. Lett. **22**, 1831 (1997).
[19] D. Hofstetter and R. L. Thornton, Appl. Phys. Lett. **72**, 404 (1998).
[20] G. Belenky, C. L. Reynolds Jr., L. Shterengas, M. S. Hybertsen, D. V. Donetsky, G. E. Shtengel, and S. Luryi, IEEE Photonics Technol. Lett. **12**, 969 (2000).
[21] L. Thylen, IEEE J. Quantum Electron. **24**, 1532 (1988).
[22] I. P. Kaminow, G. Eisenstein, and L. W. Stulz, IEEE J. Quantum Electron. **19**, 493 (1983).
[23] J. Piprek, P. Abraham, and J. E. Bowers, IEEE J. Quantum Electron. **36**, 366 (2000).
[24] C. M. Kim, J. Cho, J. Lee, S. Rim, S. H. Lee, K. R. Oh, and J. H. Kim, Appl. Phys. Lett. **92**, 131110 (2008).
[25] M. Hentschel and H. Schomerus, Phys. Rev. E **65**, 045603 (2002).
[26] R. C. Polson, G. Levina, and Z. V. Vardeny, Appl. Phys. Lett. **76**, 3858 (2000).
[27] M. Born and E. Wolf, *Principles of Optics* (Cambridge University Press, Cambridge, 1999).
[28] J. Piprek, P. Abraham, and J. E. Bowers, IEEE J. Sel. Top. Quantum Electron. **5**, 643 (1999).